Editors' Suggestion | Featured in Physics

Lamellar to Micellar Phases and Beyond: When Tactic Active Systems Admit Free Energy Functionals

J. O'Byrne and J. Tailleur
Université de Paris, Laboratoire Matière et Systèmes Complexes (MSC), UMR 7057 CNRS, F-75205 Paris, France

(Received 7 July 2020; accepted 14 October 2020; published 13 November 2020; corrected 9 April 2021)

We consider microscopic models of active particles whose velocities, rotational diffusivities, and tumbling rates depend on the gradient of a local field that is either externally imposed or depends on all particle positions. Despite the fundamental differences between active and passive dynamics at the microscopic scale, we show that a large class of such tactic active systems admit fluctuating hydrodynamics equivalent to those of interacting Brownian colloids in equilibrium. We exploit this mapping to show how taxis may lead to the lamellar and micellar phases observed for soft repulsive colloids. In the context of chemotaxis, we show how the competition between chemoattractant and chemorepellent may lead to a bona fide equilibrium liquid-gas phase separation in which a loss of thermodynamic stability of the fluid signals the onset of a chemotactic collapse.

DOI: 10.1103/PhysRevLett.125.208003

Over the past ten years, the development of a wealth of synthetic active systems has paved the way for engineering active materials [1–9]. Unlike in equilibrium, however, there is no guiding principle for the self-assembly of active systems due to the lack of a generic expression for their steady states. A natural way forward that has been heavily investigated recently [10–17] is to determine to what extent the knowledge we have garnered in—and close to—equilibrium remains relevant to active matter. A first positive answer is provided by the wealth of works on effective temperatures in active systems [18–23], which show that an effective fluctuation-dissipation relation may, under some conditions, survive activity. Then, similarities between active and passive dynamics have also been detected at the level of collective behaviors [24–27]. For instance, the interplay between self-propulsion and repulsive forces leads to a motility-induced phase separation (MIPS) that is only observed far from equilibrium at large propulsion velocities [28]. Nevertheless, from the equality of pressures in coexisting phases to its coarsening dynamics, MIPS shares several features, at the macroscopic scale, with an equilibrium liquid-gas phase separation [10–13,29–31]. Two natural questions, then, are how general is this meso- to large-scale similarity between active and passive dynamics and under which conditions, if any, does the microscopic driving out of equilibrium of active particles disappears upon coarse graining [32]?

Among the physical phenomena that control active dynamics, taxis plays an important role in a large range of situations [33]. It is widespread in the biological world—from the chemotaxis of run-and-tumble bacteria [34] to the phototaxis of algae [35] through the durotaxis of cells [36]. Taxis is not limited, however, to living systems. Self-propelled colloids often rely on the presence of chemicals in their environment to power their self-propulsion [1] that also bias their dyamics [37,38]. Taxis is known to lead to rich, system-specific behaviors that occur at the microscopic and collective levels [37–45]. While some of these phenomena are nonequilibrium in nature [42,44,46–48], the aforementioned connections between active systems and equilibrium physics raise the question as to whether microscopic tactic dynamics may also lead to emerging behaviors described by coarse-grained equilibrium theories.

In this Letter, we answer this question for a broad class of active particles, which we refer to as 'tactic active particles' (TAPs), whose propelling speeds or orientational dynamics are biased by the gradients of a field $c(\boldsymbol{r}, t)$. Using a diffusive scaling of time and space, we construct their fluctuating hydrodynamics and determine under which conditions the latter satisfy detailed balance, whence admitting a free-energy functional. This allows us to reveal a one-to-one correspondence, at this coarse-grained level, between tactic active particles and interacting Brownian colloids. Despite the fundamental differences between these two systems at the microscopic scales, a mapping may thus exist between the large-scale dynamics and steady-state statistics of their density fields. We then exploit this result to report the existence of the micellar and lamellar phases usually observed for softly repulsive Brownian colloids. In the context of chemotaxis, we further show how the competition between chemoattractant and chemorepellent can be rationalized using the physics of Brownian colloids undergoing a liquid-gas phase separation. A simple criterion is then proposed to predict the onset of a chemotactic collapse, which amounts to a loss of

thermodynamic stability of the fluid phase. Finally, we show that externally imposed chemical fields $c(\boldsymbol{r})$ map onto external potentials in equilibrium.

We consider N self-propelled particles whose positions evolve as

$$\dot{\boldsymbol{r}}_i = v_p \boldsymbol{u}_i + \sqrt{2D_t}\boldsymbol{\eta}_i, \tag{1}$$

where $\boldsymbol{u}_i$ is a unit vector indicating the orientation of particle i, v_p is its self-propulsion speed, and $\{\boldsymbol{\eta}_i\}$ forms a set of N Gaussian white noises whose spatial components satisfy $\langle \eta_i^a(t)\eta_j^b(t')\rangle = \delta^{ab}\delta_{ij}\delta(t-t')$. The particles' orientations evolve through rotational diffusion (in $d>1$ dimensions) and instantaneous tumbles. To model taxis, we consider two possible couplings between the field c and the active dynamics. First, the speed of a particle may depend on its orientation with respect to ∇c through a linear coupling

$$v_p = v_0 - v_1 \boldsymbol{u}_i \cdot \nabla c. \tag{2}$$

Alternatively, taxis may stem from the anisotropy of the orientational dynamics. We model the latter as direction-dependent tumbling rate α and rotational diffusivity Γ [49]:

$$\alpha = \alpha_0 + \alpha_1 \boldsymbol{u}_i \cdot \nabla c \quad \text{and} \quad \Gamma = \Gamma_0 + \Gamma_1 \boldsymbol{u}_i \cdot \nabla c. \tag{3}$$

Positive values of v_1, α_1, and Γ_1 drive the particles toward lower values of c [50].

Experimentally, Eq. (2) can be implemented using feedback loops [51,52] when the speed of self-propelled particles can be controlled by light—a class that comprises both Janus colloids [5,51,53] and bacteria [54–57]. The field $c(\boldsymbol{r}, \{\boldsymbol{r}_i\})$ can then be an arbitrary function of all particle positions. Equation (3) is also a standard model for the chemotaxis of run-and-tumble bacteria [34,41,47,58]. The field $c(\boldsymbol{r})$ then models a chemorepellent ($\alpha_1 > 0$) or a chemoattractant ($\alpha_1 < 0$), which can be either produced by the bacteria or imposed externally. To cover both cases, we consider the many-body dynamics in which $c(\boldsymbol{r}_i, [\rho])$ is both a function of $\boldsymbol{r}_i$ and a functional of the particle density. In the context of diffusing fields, this amounts to integrating out the dynamics of the chemotactic fields, following, e.g., [37,38].

Fluctuating mesoscopic description.—While much insight can be gained from deterministic hydrodynamic descriptions of active systems [47,59–61], measuring their irreversibility by, say, computing entropy production requires working at the fluctuating level. At scales much larger than their persistence length, noninteracting active random walks lead to diffusive behaviors [62,63]. We thus rescale space and time as $(x,t) \to (x/L, t/L^2)$, where L is the linear size of the system, and study the fate of interacting TAPs under this scaling. To proceed, we average out the orientational degrees of freedom in the spirit of [10,25,58,64–66]. To lighten the notations, we focus for now on rotational diffusion. The N-body probability density $\psi(\{\boldsymbol{r}_i, \boldsymbol{u}_i\}, t)$ then evolves as

$$\partial_t \psi = -L \sum_{i=1}^{N} \nabla_{\boldsymbol{r}_i} \cdot \left[\left(v_0 - \frac{v_1}{L} \boldsymbol{u}_i \cdot \nabla_{\boldsymbol{r}_i} c \right) \boldsymbol{u}_i \psi - \frac{D_t}{L} \nabla_{\boldsymbol{r}_i} \psi \right] + L^2 \sum_i \Delta_{\boldsymbol{u}_i} \left[\left(\Gamma_0 + \frac{\Gamma_1}{L} \boldsymbol{u}_i \cdot \nabla_{\boldsymbol{r}_i} c \right) \psi \right]. \tag{4}$$

Integrating over all orientational degrees of freedom leads to a conservation equation $\partial_t \phi(\{\boldsymbol{r}_i\}, t) = -\sum_i \nabla_{\boldsymbol{r}_i} \cdot \boldsymbol{J}_i(\{\boldsymbol{r}_i\}, t)$, where $\boldsymbol{J}_i \equiv -D_t \nabla_{\boldsymbol{r}_i} \phi + \int \Pi_j \mathrm{d}\boldsymbol{u}_j (v_0 L - v_1 \boldsymbol{u}_i \cdot \nabla_{\boldsymbol{r}_i} c) \boldsymbol{u}_i \psi$ is the probability current along direction $\boldsymbol{r}_i$ and ϕ is the marginal in space of ψ. To compute the diffusive limit of $\boldsymbol{J}_i$, the dynamics, Eq. (4), can be projected onto its successive N-body harmonics, leading to a hierarchy of equations [67]. Under the assumption of a lack of long-range correlations between the particle orientations, a closure is obtained by noticing that all moments beyond $\phi(\{\boldsymbol{r}_i\}, t)$ are fast fields and decay as $1/L$ (or faster) in the large system-size limit, leading to

$$\boldsymbol{J}_i \simeq -\left(D_t + \frac{v_0^2}{d(d-1)\Gamma_0} \right) \nabla_{\boldsymbol{r}_i} \phi - \phi \left[\frac{\nabla_{\boldsymbol{r}_i} v_0^2}{2d(d-1)\Gamma_0} + \left(\frac{v_0 \Gamma_1 + v_1 \Gamma_0}{d\Gamma_0} \right) \nabla_{\boldsymbol{r}_i} c \right]. \tag{5}$$

At this stage, we have constructed a coarse-grained diffusive description of the dynamics given by Eq. (1)–(3). We now restore, for full generality, the possibility of tumbles and take v_i, α_i, and Γ_i constant to focus on the consequences of taxis. Using stochastic calculus, one then obtains a corresponding fluctuating hydrodynamics for the density field $\rho(\boldsymbol{r}) = \sum_{i=1}^{N} \delta(\boldsymbol{r} - \boldsymbol{r}_i)$:

$$\partial_t \rho = -\nabla \cdot [J_D + \sqrt{2D\rho}\Lambda] \tag{6}$$

$$J_D = -D\rho\nabla \left\{ \log\rho + \left[v_1 + v_0 \frac{\alpha_1 + (d-1)\Gamma_1}{\alpha_0 + (d-1)\Gamma_0} \right] \frac{c}{dD} \right\}, \tag{7}$$

where $\Lambda(\boldsymbol{r}, t)$ is a Gaussian noise field of zero mean and correlations $\langle \Lambda(\boldsymbol{r}, t)\Lambda(\boldsymbol{r}', t')\rangle = \delta(t-t')\delta(\boldsymbol{r}-\boldsymbol{r}')$, J_D is the deterministic part of the current, and D is a large-scale diffusivity:

$$D = D_t + \frac{v_0^2}{d[\alpha_0 + (d-1)\Gamma_0]}. \tag{8}$$

Equations (6) and (7) describe the stochastic dynamics of the density field of TAPs at scales much larger than their persistence lengths and times and can now be used to study their emerging collective behaviors.

Effective free-energy functionals.—Inspection of Eq. (7) shows that the deterministic part of the current can be written as $J_D = -D\rho\nabla\mu$, where μ plays the role of a nonequilibrium chemical potential [68]. An interesting outcome of the diffusive scaling is that the noise field and the mobility appearing in J_D satisfy a generalized Stokes–Einstein relation. The dynamics, Eq. (6), then satisfies detailed balance whenever one can find a free energy $\mathcal{F}[\rho]$ whose functional derivative is given by μ.

The solution of such an inverse variational problem [69] can be obtained by generalizing the Schwarz condition of integrability to functional integration. In practice, we introduce

$$\mathcal{D}(\boldsymbol{r},\boldsymbol{r}') = \frac{\delta\mu([\rho],\boldsymbol{r})}{\delta\rho(\boldsymbol{r}')} - \frac{\delta\mu([\rho],\boldsymbol{r}')}{\delta\rho(\boldsymbol{r})}, \tag{9}$$

which is such that $\mu(\boldsymbol{r},[\rho])$ is a functional derivative iff for any two test functions f, g [70],

$$\int \mathcal{D}(\boldsymbol{r},\boldsymbol{r}')f(\boldsymbol{r})g(\boldsymbol{r}')d\boldsymbol{r}d\boldsymbol{r}' = 0. \tag{10}$$

Note that Eq. (10) means that $\mathcal{D}$ vanishes as a distribution, which is not always straightforward to read in its expression. For instance, in one dimension, $\mu = \partial_x^k\rho$ leads to $\mathcal{D}(x,x') = (\partial_x^k - \partial_{x'}^k)\delta(x-x')$; μ admits a functional integral iff k is even, which can be checked easily using Eq. (10).

Let us now consider a field c given by

$$c([\rho],\boldsymbol{r}) = \int K(\boldsymbol{r},\boldsymbol{r}_1,\ldots,\boldsymbol{r}_{p-1})\rho(\boldsymbol{r}_1),\ldots, \times\rho(\boldsymbol{r}_{p-1})d\boldsymbol{r}_1,\ldots,d\boldsymbol{r}_{p-1}. \tag{11}$$

Equation (10) is satisfied whenever the kernel K is invariant under any permutation of its variables. The fluctuating hydrodynamics (6)–(7) then becomes

$$\partial_t\rho = \nabla\cdot\left[D\rho\nabla\frac{\delta\mathcal{F}}{\delta\rho} - \sqrt{2D\rho}\Lambda\right], \tag{12}$$

where the effective free-energy functional $\mathcal{F}$ is given by

$$\mathcal{F}[\rho] = \int d\boldsymbol{r}\rho(\boldsymbol{r})\log\rho(\boldsymbol{r}) + \frac{v_0}{dD}\left[\frac{v_1}{v_0} + \frac{\alpha_1+(d-1)\Gamma_1}{\alpha_0+(d-1)\Gamma_0}\right] \times\frac{1}{p!}\int K(\boldsymbol{r}_1,\ldots,\boldsymbol{r}_p)\rho(\boldsymbol{r}_1),\ldots,\rho(\boldsymbol{r}_p)d\boldsymbol{r}_1,\ldots,d\boldsymbol{r}_p. \tag{13}$$

Importantly, Eqs. (12) and (13) also describe the fluctuating hydrodynamics of N Brownian colloids interacting via a p-body potential. More precisely, consider N particles undergoing the equilibrium Langevin dynamics

$$\gamma\dot{\boldsymbol{r}}_i = -\sum_{j_1<\ldots<j_{p-1}}\nabla_{\boldsymbol{r}_i}V(\boldsymbol{r}_i,\boldsymbol{r}_{j_1},\ldots,\boldsymbol{r}_{j_{p-1}}) + \sqrt{2\gamma T}\boldsymbol{\eta}, \tag{14}$$

where we have introduced a temperature T, a damping γ, and a p-body potential V. Equations (12) and (13) describe the fluctuating hydrodynamics of this system upon identifying

$$\gamma^{-1}T \Leftrightarrow D$$
$$\gamma^{-1}V(\boldsymbol{r}_1,\ldots,\boldsymbol{r}_p) \Leftrightarrow \left[\frac{v_1}{d} + \frac{v_0}{d}\frac{\alpha_1+(d-1)\Gamma_1}{\alpha_0+(d-1)\Gamma_0}\right]K(\boldsymbol{r}_1,\ldots,\boldsymbol{r}_p). \tag{15}$$

The mapping, Eq. (15), establishes a macroscopic connection between the nonequilibrium dynamics, Eqs. (1)–(3), and the equilibrium dynamics, Eq. (14), which strongly differ at the microscopic scale. In particular, the roles played by K and V in these microscopic dynamics are of very different natures, despite their similar role in the macroscopic dynamics of ρ. This differs from approaches in which the chemotaxis of cells is already modeled at the microscopic level by Brownian dynamics in which the field c plays the role of a potential [71]. The macroscopic equivalence described there with equilibrium dynamics directly stems from a microscopic one. Note that, while a similarity between active and passive collective behaviors has been reported in the case of MIPS [10–13,29–31], the mapping, Eq. (15), suggests a much broader relationship between passive and active systems, which we now explore.

Micellar, lamellar, and crystalline phases.—The recent development of active systems in which the particle velocities can be controlled individually using light [51,52] makes the realization of dynamics, Eqs. (1)–(2), within experimental reach. Once the particle density has been measured, their velocities can be set according to Eq. (2) by adjusting the light field, where $c(\boldsymbol{r})$ is obtained from $\rho(\boldsymbol{r})$ using Eq. (11) and an arbitrary kernel K. To explore the physics these systems can access, we consider a convolution kernel $K(\boldsymbol{r},\boldsymbol{r}_1) = K(\boldsymbol{r}-\boldsymbol{r}_1)$ with two typical length scales:

$$K(\boldsymbol{r}) = Ae^{-[\sigma_0^2/(\sigma_0^2-r^2)]}\Theta(\sigma_0-|\boldsymbol{r}|) + \epsilon e^{-[\sigma_1^2/\sigma_1^2-r^2]}\Theta(\sigma_1-|\boldsymbol{r}|), \tag{16}$$

where $\Theta(u)$ is the Heaviside function and we consider $A > \epsilon$ and $\sigma_1 > \sigma_0$. We report in the top row of Fig. 1 simulations of the active dynamics, Eqs. (1)–(2). As the density increases, the system undergoes a series of phase transitions: a disordered gas (not shown) is first replaced by a crystal of "micelles," each comprising an increasing number of particles as the density increases (1st column), until a laning transition occurs. Further increasing the density increases the local number of particles forming the lanes (2nd and 3rd columns). At higher densities,

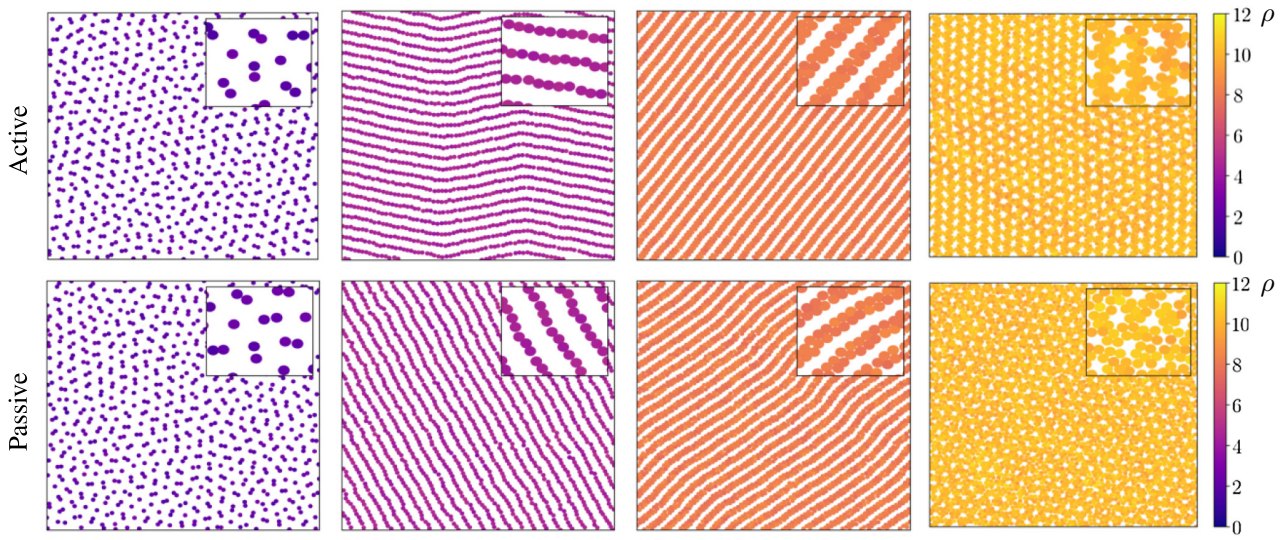

FIG. 1. Simulations of dynamics, Eqs. (1)–(2), (top) and of the equilibrium dynamics, Eq. (14), (bottom) under the conditions of the mapping, Eq. (15), with $K(\boldsymbol{r})$ defined by Eq. (16). Color encodes the local density. Parameters: $v_0 = 1$, $v_1 = 0.2$, $\alpha_0 = 50$, $\sigma_0 = 0.3$, $\sigma_1 = 1$, $\varepsilon = 5$, $A = 10$, $D_t = \alpha_1 = \Gamma_i = 0$, $dt = 10^{-3}$. Snapshots taken at $t = 20000$ in a system of size 20×20. From left to right, $\rho_0 \equiv N/L^2$ is equal to 2, 4, 8, and 10.

inverted crystals develop, in which voids and particles have exchanged their previous roles (4th column). The underlying physics can be rationalized thanks to our equilibrium mapping: simulations of the passive dynamics, Eq. (14), for parameters satisfying Eq. (15) indeed perfectly match those of TAPs (Fig. 1, bottom row). In the passive picture, the kernel, Eq. (16), corresponds to a pairwise potential with a repulsive central core and a softer repulsive shoulder. Using equilibrium Monte Carlo simulations, similar potentials have been shown to lead to a variety of exotic phases [72–74], which are thus accessible to TAPS.

Chemotaxis: competition between attraction and repulsion.—While fields $c(\boldsymbol{r}, [\rho])$ given by Eq. (11) can be engineered in the lab, they can also be found in nature. In biological systems, tactic interactions are often mediated by diffusing molecules, which naturally lead to a linear coupling between ρ and c. Interactions mediated by fluctuating membranes or interfaces would lead to nonlinearities that offer an interesting (and challenging) problem for future works. Inspired by bacterial chemotaxis, we consider a model system in which active particles interact through the production of a chemoattractant and a chemorepellent. Introducing their concentration fields c_a and c_r, we write the tumbling rate of particle i as $\alpha = \alpha_0 - \alpha_1^a \boldsymbol{u}_i \cdot \nabla c_a + \alpha_1^r \boldsymbol{u}_i \cdot \nabla c_r$. Taking $\alpha_1^r > 0$ and $\alpha_1^a > 0$, then bias the random walk of particle i toward high-c_a regions and away from high-c_r regions.

After their production by the particles, at rates $a_{a,r}$, the signaling molecules diffuse with diffusivity $\nu_{a,r}$ and are degraded at rates $\lambda_{a,r}$, leading to the dynamics

$$\partial_t c_n(\boldsymbol{r}) = \nu_n \Delta c_n(\boldsymbol{r}) - \lambda_n c_n + a_n \sum_i \delta(\boldsymbol{r} - \boldsymbol{r}_i), \tag{17}$$

where $n \in \{a, r\}$. A standard, fast variable treatment on c_n then leads to the screened Poisson equation

$$\left(\Delta - \frac{\lambda_n}{\nu_n}\right) c_n = -\frac{a_n}{\nu_n}\rho, \tag{18}$$

which can be solved as $c_n = (a_n/\nu_n) G_n * \rho$, where G_n is the Green function of Eq. (18). The system thus satisfies the mapping condition, Eq. (11), with $p = 2$. Introducing the screening lengths $\ell \equiv \sqrt{\nu_n/\lambda_n}$, the Green functions are given by $G_n(\boldsymbol{r}) = \ell_n e^{-|\boldsymbol{r}|/\ell_n}/2$ in 1D, $G_n(\boldsymbol{r}) = K_0(|\boldsymbol{r}|/\ell_n)/2\pi$ in 2D, where K_0 is the 0th order modified Bessel function of the second kind, and $K(\boldsymbol{r}) = e^{-|\boldsymbol{r}|/\ell_n}/4\pi|\boldsymbol{r}|$ in 3D. The mapping, Eq. (15), then shows this system of active particles to be equivalent at the fluctuating hydrodynamic level to passive Brownian particles interacting via a pair potential

$$V(\boldsymbol{r}) = \frac{\gamma v_0}{d\alpha_0}\left[\alpha_1^r \frac{a_r}{\nu_r} G_r(\boldsymbol{r}) - \alpha_1^a \frac{a_a}{\nu_a} G_a(\boldsymbol{r})\right]. \tag{19}$$

The superposition of chemoattractant and chemorepellent thus directly maps onto an equilibrium problem with attractive and repulsive interactions. Let us consider the case in which $\alpha_1^r > \alpha_1^a$ and $\ell_r \leq \ell_a$. The physics of this chemotactic system is now mapped onto the well-known problem of repulsive hard-core interactions with attractive tails. The system is purely repulsive for $\ell_a = \ell_r$, hence

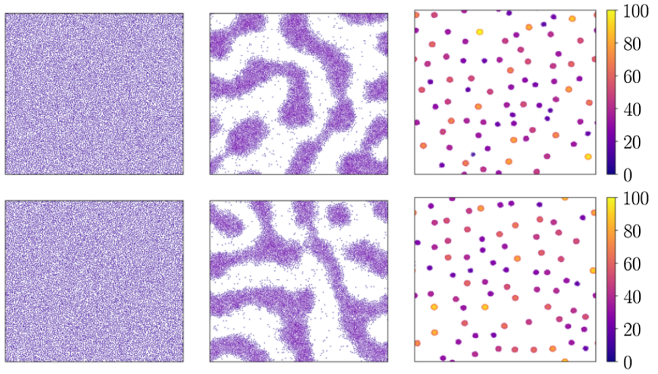

FIG. 2. Simulations of the active dynamics, Eqs. (1)–(3), top, and the equilibrium dynamics, Eq. (14), bottom, using the pair potential, Eq. (19), under the conditions of the mapping, Eq. (15). Color encodes the local density. From left to right $\ell_r = 1/6$, $1/8, 1/10$. Chemotactic collapse is predicted when $\bar{V} < 0$, i.e., below $\ell_r = 1/8.2$. Parameters: $L = 40$, $\rho_0 = 7$, $a_a/2\pi\nu_a = 0.05$, $\ell_a = 0.25$, $a_r/2\pi\nu_r = 0.2$, $\alpha_0 = 100$, $\alpha_1^{r,a} = 200$, $v_0 = 1$, $T^{-1} = 200$, $\gamma = 1$, $v_1 = \Gamma_i = D_t = 0$, $dt = 10^{-3}$. The snapshots were taken after a time $t = 10^4$.

leading to a gas phase. As ℓ_r decreases, the attractive tail develops, allowing for a liquid-gas coexistence. For even shorter ℓ_r, the liquid phase becomes thermodynamically unstable, leading to a collapse of the system when $\bar{V} \equiv \int d\boldsymbol{r} V(\boldsymbol{r}) < 0$ [75]. Figure 2 compares simulations of the passive dynamics, Eq. (14), and the active dynamics, Eqs. (1)–(3), using the 2D Green functions of Eq. (18) as ℓ_r is varied. Once again, despite the fundamental differences between their microscopic dynamics and interactions, the large-scale physics of these two systems is hardly distinguishable.

External fields.—Finally, while we have focused so far on collective effects, nothing prevents an additional taxis toward an externally controlled field $w(\boldsymbol{r})$. Our models of taxis, Eqs. (2) and (3), are easily generalized to this case, using, for instance,

$$\begin{cases} v_p &= v_0 - v_1 \boldsymbol{u}_i \cdot \nabla c - v_2 \boldsymbol{u}_i \cdot \nabla w \\ \alpha &= \alpha_0 + \alpha_1 \boldsymbol{u}_i \cdot \nabla c + \alpha_2 \boldsymbol{u}_i \cdot \nabla w \\ \Gamma &= \Gamma_0 + \Gamma_1 \boldsymbol{u}_i \cdot \nabla c + \Gamma_2 \boldsymbol{u}_i \cdot \nabla w, \end{cases} \tag{20}$$

where the field c still accounts for interactions between the self-propelled particles given by Eq. (11). The equilibrium mapping still holds, with a free energy now given by

$$\tilde{\mathcal{F}}[\rho] = \mathcal{F}[\rho] + \frac{v_0}{dD}\left[\frac{v_2}{v_0} + \frac{\alpha_2 + (d-1)\Gamma_2}{\alpha_0 + (d-1)\Gamma_0}\right] \int d\boldsymbol{r} w(\boldsymbol{r}) \rho(\boldsymbol{r}),$$

where $\mathcal{F}$ remains given by Eq. (13). The external field $w(\boldsymbol{r})$ is thus equivalent to an external potential for Brownian colloids. Much like gravity, it can be used to localize a dense phase in a phase-separated system.

Discussion.—The mapping between TAPS and Brownian colloids presented in this Letter offers an interesting route to control synthetic active matter—for instance, to prepare a desired initial condition in a light-controlled active system [51,52]. It also offers a qualitative insight into the large-scale behaviors of tactic active particles, which, as for MIPS, should hold beyond the sole systems that will obey exactly the dynamics, Eqs. (1)–(3).

The derivation of Eq. (5), detailed in the Supplemental Material [67], works directly at the interacting N-body level. This differs from standard treatments of chemotaxis that rely on an explicit dynamics of the field c, assumed to be slow, to work at an essentially noninteracting level [76]. Our treatment relies on a lack of long-range orientational order and precludes, in particular, large-scale collective motion. Whether the latter may emerge in a setting as simple as the one described by Eqs. (1)–(3) is an open, challenging question, stimulated in particular by the works on bacterial traveling waves [42,47]. Furthermore, our derivation assumes that the field gradients remain finite, which has to be checked self-consistently. In particular, it certainly does not hold in the late-stage dynamics of the chemotactic collapse reported in Fig. 2, which only highlights the remarkable agreement between passive and active dynamics in this case.

In this Letter, we have focused on active systems whose large-scale dynamics obey detailed balance, but the interest of our mapping is not limited to these cases. Studying the linear response to fields violating Eq. (10) or (15) is a natural next step. Near-equilibrium studies of active matter models have indeed been shown to capture many interesting properties of active systems [77–80]. Furthermore, the approach to the inverse variational problem described in Eqs. (9)–(10) can easily be generalized to more complex situations—for instance, involving several species of active particles [44,81–83].

Finally, we have focused on the consequences that the mapping, Eq. (15), bears on the steady-state distributions of tactic active systems. The one-to-one correspondence is established, however, at a dynamical level, as illustrated by videos 1 and 2 in the Supplemental Material [67]. This paves the way toward studying the transition states of tactic active systems using methods like transition path sampling [84] or the string method [85].

The authors benefited from participation in the 2020 KITP program on Active Matter supported by the grant NSF PHY-1748958.

[1] J. R. Howse, R. A. L. Jones, A. J. Ryan, T. Gough, R. Vafabakhsh, and R. Golestanian, Phys. Rev. Lett. **99**, 048102 (2007).

[2] J. Palacci, C. Cottin-Bizonne, C. Ybert, and L. Bocquet, Phys. Rev. Lett. **105**, 088304 (2010).

[3] S. Thutupalli, R. Seemann, and S. Herminghaus, New J. Phys. **13**, 073021 (2011).
[4] A. Bricard, J.-B. Caussin, N. Desreumaux, O. Dauchot, and D. Bartolo, Nature (London) **503**, 95 (2013).
[5] J. Palacci, S. Sacanna, A. P. Steinberg, D. J. Pine, and P. M. Chaikin, Science **339**, 936 (2013).
[6] D. Nishiguchi and M. Sano, Phys. Rev. E **92**, 052309 (2015).
[7] J. Yan, M. Han, J. Zhang, C. Xu, E. Luijten, and S. Granick, Nat. Mater. **15**, 1095 (2016).
[8] C. Bechinger, R. Di Leonardo, H. Löwen, C. Reichhardt, G. Volpe, and G. Volpe, Rev. Mod. Phys. **88**, 045006 (2016).
[9] P. G. Moerman, H. W. Moyses, E. B. Van Der Wee, D. G. Grier, A. Van Blaaderen, W. K. Kegel, J. Groenewold, and J. Brujic, Phys. Rev. E **96**, 032607 (2017).
[10] J. Tailleur and M. E. Cates, Phys. Rev. Lett. **100**, 218103 (2008).
[11] T. Speck, J. Bialké, A. M. Menzel, and H. Löwen, Phys. Rev. Lett. **112**, 218304 (2014).
[12] S. C. Takatori, W. Yan, and J. F. Brady, Phys. Rev. Lett. **113**, 028103 (2014).
[13] F. Ginot, I. Theurkauff, D. Levis, C. Ybert, L. Bocquet, L. Berthier, and C. Cottin-Bizonne, Phys. Rev. X **5**, 011004 (2015).
[14] U. M. B. Marconi, C. Maggi, and S. Melchionna, Soft Matter **12**, 5727 (2016).
[15] J. Rodenburg, M. Dijkstra, and R. van Roij, Soft Matter **13**, 8957 (2017).
[16] A. P. Solon, J. Stenhammar, M. E. Cates, Y. Kafri, and J. Tailleur, Phys. Rev. E **97**, 020602(R) (2018).
[17] E. Flenner and G. Szamel, Phys. Rev. E **102**, 022607 (2020).
[18] D. Loi, S. Mossa, and L. F. Cugliandolo, Phys. Rev. E **77**, 051111 (2008).
[19] S. Wang and P. G. Wolynes, J. Chem. Phys. **135**, 051101 (2011).
[20] D. Loi, S. Mossa, and L. F. Cugliandolo, Soft Matter **7**, 3726 (2011).
[21] K. I. Morozov and L. M. Pismen, Phys. Rev. E **81**, 061922 (2010).
[22] G. Szamel, Phys. Rev. E **90**, 012111 (2014).
[23] A. P. Solon, M. Cates, and J. Tailleur, Eur. Phys. J. Special Topics **224**, 1231 (2015).
[24] P. Chavanis, M. Ribot, C. Rosier, and C. Sire, Banach Cent. Pub. **66**, 287 (2004), http://eudml.org/doc/282071.
[25] R. Golestanian, Phys. Rev. Lett. **108**, 038303 (2012).
[26] S. C. Takatori and J. F. Brady, Phys. Rev. E **91**, 032117 (2015).
[27] S. Paliwal, J. Rodenburg, R. van Roij, and M. Dijkstra, New J. Phys. **20**, 015003 (2018).
[28] M. E. Cates and J. Tailleur, Annu. Rev. Condens. Matter Phys. **6**, 219 (2015).
[29] A. G. Thompson, J. Tailleur, M. E. Cates, and R. A. Blythe, J. Stat. Mech. (2011), P02029 (2011).
[30] D. Bi, X. Yang, M. C. Marchetti, and M. L. Manning, Phys. Rev. X **6**, 021011 (2016).
[31] T. Grafke, M. E. Cates, and E. Vanden-Eijnden, Phys. Rev. Lett. **119**, 188003 (2017).
[32] C. Nardini, É. Fodor, E. Tjhung, F. Van Wijland, J. Tailleur, and M. E. Cates, Phys. Rev. X **7**, 021007 (2017).
[33] Taxis describes the biased motion of an entity in response to an external signal.
[34] H. C. Berg, *E. coli in Motion* (Springer Science & Business Media, New York, 2008).
[35] M. Polin, I. Tuval, K. Drescher, J. P. Gollub, and R. E. Goldstein, Science **325**, 487 (2009).
[36] R. Sunyer, V. Conte, J. Escribano, A. Elosegui-Artola, A. Labernadie, L. Valon, D. Navajas, J. M. García-Aznar, J. J. Muñoz, P. Roca-Cusachs *et al.*, Science **353**, 1157 (2016).
[37] R. Soto and R. Golestanian, Phys. Rev. Lett. **112**, 068301 (2014).
[38] O. Pohl and H. Stark, Phys. Rev. Lett. **112**, 238303 (2014).
[39] D. Woodward, R. Tyson, M. Myerscough, J. Murray, E. Budrene, and H. Berg, Biophys. J. **68**, 2181 (1995).
[40] M. P. Brenner, L. S. Levitov, and E. O. Budrene, Biophys. J. **74**, 1677 (1998).
[41] S. Chatterjee, R. A. da Silveira, and Y. Kafri, PLoS Comput. Biol. **7**, e1002283 (2011).
[42] J. Saragosti, V. Calvez, N. Bournaveas, B. Perthame, A. Buguin, and, P. Silberzan, Proc. Natl. Acad. Sci. U.S.A. **108**, 16235 (2011).
[43] S. Saha, R. Golestanian, and S. Ramaswamy, Phys. Rev. E **89**, 062316 (2014).
[44] J. Agudo-Canalejo and R. Golestanian, Phys. Rev. Lett. **123**, 018101 (2019).
[45] B. Nasouri and R. Golestanian, Phys. Rev. Lett. **124**, 168003 (2020).
[46] R. E. Goldstein, Phys. Rev. Lett. **77**, 775 (1996).
[47] M. Seyrich, A. Palugniok, and H. Stark, New J. Phys. **21**, 103001 (2019).
[48] S. Mahdisoltani, R. B. A. Zinati, C. Duclut, A. Gambassi, and R. Golestanian,arXiv:1911.08115.
[49] The rotational diffusion is understood as an Itō–Langevin process.
[50] The sign conventions in Eqs. (1)–(3) are chosen to make the mapping between active and passive systems detailed below as simple as possible.
[51] T. Bäuerle, A. Fischer, T. Speck, and C. Bechinger, Nat. Commun. **9**, 3232 (2018).
[52] F. A. Lavergne, H. Wendehenne, T. Bäuerle, and C. Bechinger, Science **364**, 70 (2019).
[53] I. Buttinoni, J. Bialké, F. Kümmel, H. Löwen, C. Bechinger, and T. Speck, Phys. Rev. Lett. **110**, 238301 (2013).
[54] G. Vizsnyiczai, G. Frangipane, C. Maggi, F. Saglimbeni, S. Bianchi, and R. Di Leonardo, Nat. Commun. **8**, 15974 (2017).
[55] G. Frangipane, D. Dell'Arciprete, S. Petracchini, C. Maggi, F. Saglimbeni, S. Bianchi, G. Vizsnyiczai, M. L. Bernardini, and R. Di Leonardo, eLife **7**, e36608 (2018).
[56] J. Arlt, V. A. Martinez, A. Dawson, T. Pilizota, and W. C. Poon, Nat. Commun. **9**, 768 (2018).
[57] J. Arlt, V. A. Martinez, A. Dawson, T. Pilizota, and W. C. Poon, Nat. Commun. **10**, 2321 (2019).
[58] M. J. Schnitzer, Phys. Rev. E **48**, 2553 (1993).
[59] E. Bertin, M. Droz, and G. Grégoire, Phys. Rev. E **74**, 022101 (2006).
[60] B. Liebchen, D. Marenduzzo, and M. E. Cates, Phys. Rev. Lett. **118**, 268001 (2017).
[61] M. Kourbane-Houssene, C. Erignoux, T. Bodineau, and J. Tailleur, Phys. Rev. Lett. **120**, 268003 (2018).

[62] P. Romanczuk, M. Bär, W. Ebeling, B. Lindner, and L. Schimansky-Geier, Eur. Phys. J. Special Topics **202**, 1 (2012).
[63] M. E. Cates, Rep. Prog. Phys. **75**, 042601 (2012).
[64] C. W. Wolgemuth, Biophys. J. **95**, 1564 (2008).
[65] M. E. Cates and J. Tailleur, Europhys. Lett. **101**, 20010 (2013).
[66] A. E. Hamby, D. K. Vig, S. Safonova, and C. W. Wolgemuth, Sci. Adv. **4**, eaau0125 (2018).
[67] See Supplemental Material at http://link.aps.org/supplemental/10.1103/PhysRevLett.125.208003 for derivation and discussion of the diffusive limit of Eqs. (1)–(3) and supplemental videos.
[68] P. M. Chaikin and T. C. Lubensky, *Principles of Condensed Matter Physics* (Cambridge University Press, Cambridge, England, 1995), Vol. 10.
[69] I. M. Anderson, The variational bicomplex, Tech. Rep., Utah State Technical Report, 1989, http://math. usu. edu/ fg mp, 1989.
[70] As usual, there are topological requirements for the conditions to be sufficient [69].
[71] P.-H. Chavanis, Commun. Nonlinear Sci. Numer. Simul. **15**, 60 (2010).
[72] G. Malescio and G. Pellicane, Nat. Mater. **2**, 97 (2003).
[73] M. A. Glaser, G. M. Grason, R. D. Kamien, A. Košmrlj, C. D. Santangelo, and P. Ziherl, Europhys. Lett. **78**, 46004 (2007).
[74] H. Löwen, in *Understanding Soft Condensed Matter Via Modeling and Computation* (World Scientific, Singapore, 2011), pp. 9–45.
[75] D. Ruelle, *Statistical Mechanics: Rigorous Results* (World Scientific, Singapore, 1999).
[76] H. G. Othmer and T. Hillen, SIAM J. Appl. Math. **61**, 751 (2000).
[77] U. M. B. Marconi, N. Gnan, M. Paoluzzi, C. Maggi, and R. Di Leonardo, Sci. Rep. **6**, 1 (2016).
[78] É. Fodor, C. Nardini, M. E. Cates, J. Tailleur, P. Visco, and F. van Wijland, Phys. Rev. Lett. **117**, 038103 (2016).
[79] R. Wittmann, C. Maggi, A. Sharma, A. Scacchi, J. M. Brader, and U. M. B. Marconi, J. Stat. Mech. (2017) 113207.
[80] R. Wittmann, U. M. B. Marconi, C. Maggi, and J. M. Brader, J. Stat. Mech. (2017) 113208.
[81] R. Wittkowski, J. Stenhammar, and M. E. Cates, New J. Phys. **19**, 105003 (2017).
[82] A. I. Curatolo, N. Zhou, Y. Zhao, C. Liu, A. Daerr, J. Tailleur, and J.-D. Huang, Nat. Phys., **16**, 1152 (2020).
[83] T. Kolb and D. Klotsa, Soft Matter **16**, 1967 (2020).
[84] C. Dellago, P. G. Bolhuis, F. S. Csajka, and D. Chandler, J. Chem. Phys. **108**, 1964 (1998).
[85] E. Weinan, W. Ren, and E. Vanden-Eijnden, Phys. Rev. B **66**, 052301 (2002).

Correction: Reference [68] contained an error in the author list and has been fixed.